COMPARISON OF FRACTURE RESPONSE OF PREFLAWED TUBES UNDER INTERNAL STATIC AND DETONATION LOADING

Tong Wa Chao and **Joseph E. Shepherd**
California Institute of Technology
Graduate Aeronautical Laboratories
Pasadena, CA 91125
U.S.A.

Abstract

Fracture experiments were performed on thin-walled and preflawed aluminum 6061-T6 tubes. Flaws were machined as external axial surface notches. The tubes were 1) statically loaded with oil, 2) statically loaded with nitrogen, and 3) dynamically loaded with gaseous detonations traveling at 2.4 km/s. The experiments were controlled so that comparisons could be made on sets of specimens with the same material, tube and flaw geometry, nominal loading amplitude, and flange supports, with the only difference being the dynamics of the loading. It was found that there is a significant difference in crack propagation behavior for the three types of loading. In this paper, fracture behavior will be discussed along with the fluid dynamics involved. The tubes were also instrumented with pressure transducers, crack detection gages, and strain gages so that data on loading, crack propagating speeds, and strain history can be compared.

Nomenclature

E	Young's modulus	$\mathrm{N/m^2}$
h	shell thickness	m
ν	Poisson's ratio	
ρ	density	$\mathrm{kg/m^3}$
K_{Ic}	mode-I critical stress intensity	$\mathrm{MPa}\sqrt{\mathrm{m}}$
G_c	fracture propagation toughness	$\mathrm{J/m^2}$
d	initial notch depth	m
$2a$	initial notch length	m
L	initial notch length	m
K_s	isentropic compressibility	$\mathrm{m^2/N}$
c	sound speed	m/s
v	specific volume	$\mathrm{m^3/kg}$
P	pressure	$\mathrm{N/m^2}$
V	volume	$\mathrm{m^3}$
u	elastic energy per unit mass	J/kg
U	elastic energy	J
E	energy per unit mass	J/kg
c_v	specific heat at constant volume	J/(kg K)
c_p	specific heat at constant pressure	J/(kg K)
γ	ratio of specific heats	
s	specific entropy	J/(kg K)
R	gas constant	J/(kg K)

1 Introduction

This study is motivated by our interest in the analysis of pipe rupture in accidental explosions and the fracture-based design of explosion vessels. A key issue is the effect of loading rate on fracture threshold and fracture propagation. Fracture of a pipe due to an internal detonation wave also represents a particularly challenging type of fluid-structure interaction that has been relatively unexplored. Tubes under internal static loading were studied extensively, especially for gas transmission pipelines. Examples of work done on statically-loaded fracture of tubes include the pioneering analysis of through-wall cracked cylindrical shells by Folias (1965) and full-scale gas transmission pipeline fracture experiments by Maxey et al. (1971), Kiefner et al. (1973), and Ives et al. (1974). There are notable laboratory-scale pipe fracture experiments in conjunction with analytical and numerical efforts such as those of Emery et al. (1986) and Kobayashi et al. (1988). There are also recent computational efforts such as the one by Zhuang and O'Donoghue (2000) to simulate the fluid-structure-fracture interaction of a bursting pipe under initially static loading. The elastic response of shells to shock or detonation loading was examined by Tang (1965), Reismann (1965), de Malherbe

et al. (1966), Simkins (1987), and Thomas (2002), but these studies did not involve fracture.

In our experiments, the flaw size and geometry, tube material, and nominal loading magnitude were kept constant. The loading rate and medium were varied. One case was static rupture by hydraulic oil; another, static rupture by gaseous nitrogen at room temperature; and the third, dynamic rupture by an internal gaseous detonation. The specimen ruptured under hydraulic oil loading had the least damage. Much more substantial damage, i.e., crack propagation and plastic deformation, was observed in the cases with nitrogen and detonation loading. The nitrogen loading caused a substantially larger fracture than the detonation although the peak loading pressure was similar.

Previous similar work was done at Caltech by Beltman et al. (1999) and Beltman and Shepherd (2002) to investigate the structural response of unflawed cylindrical shells to internal shock and detonation loading. These analytical, numerical, and experimental studies demonstrated that the amplitude of the linear elastic strains are a function of both the pressure peak and the speed of the shock or detonation wave. Recent work by Chao and Shepherd (2002) studied the fracture behavior, strain response, and fracture surfaces of aluminum tubes under detonation loading with various flaw sizes.

2 Experimental Setup

2.1 Specimens

The specimens were thin-walled, seamless aluminum 6061-T6 tube. The surface notch was oriented axially, located in the middle of the tube length, and cut by a CNC machine using a jeweler's slotting saw. The notch depth (0.56 mm), notch width (0.2 mm), tube size (0.89 mm in wall thickness, 41.28 mm in outer diameter, 0.610 m long), and notch length ($L = 25.4$ mm) were the same for all tests. Figure 1 shows the geometry of the flaw. $R_{saw} = 19$ mm is the radius of the jeweler's slotting saw.

K_{Ic} (Static)	30 MPa$\sqrt{\text{m}}$
ρ	2780 kg/m^3
E	69 GPa
ν	0.33

Table 1: Aluminum 6061-T6 properties

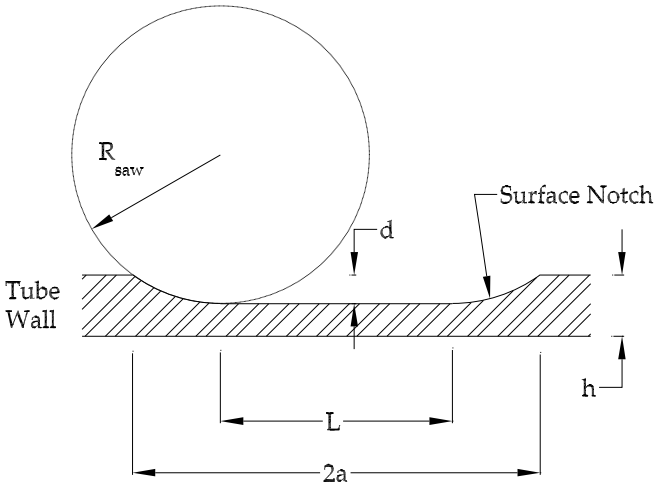

Figure 1: Flaw geometry.

2.2 Detonation Tube Assembly

Figure 2 shows a schematic of the experimental setup for the detonation loading. Figure 3 is a corresponding photograph showing the assembly aligned and bolted to aluminum plates, which were bolted to a plywood table. The setup consisted of a thick-walled detonation tube connected to the specimen tube by a flange. The tubes were sealed at one end by a flange containing the spark plug, and the other end by a Mylar diaphragm. Inside the detonation tube, a spark first created a flame, which then transitioned to a detonation wave after being accelerated through a Shchelkin spiral. The detonation wave propagated into the specimen tube. The Mylar diaphragm is burst by the detonation so that the effects of a reflected shock wave were minimized. Pressure transducers mounted on the detonation tube measured the pressure profile and wave speeds.

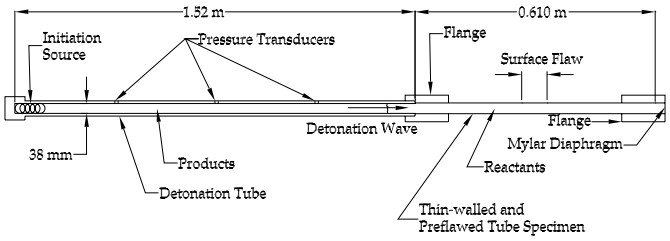

Figure 2: Tube assembly schematic for detonation experiment.

For the gaseous nitrogen and hydraulic oil loading experiments, the setup is shown in Fig. 4. The specimen tube was connected to the same flanges used in the detonation exper-

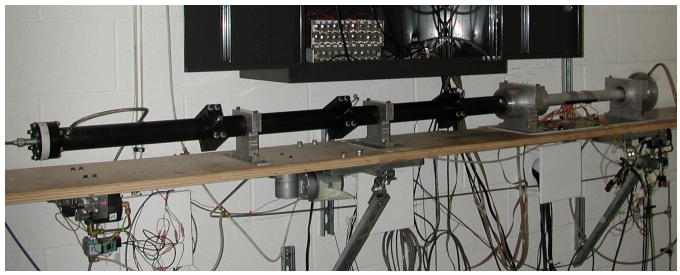

Figure 3: Tube assembly for detonation experiment.

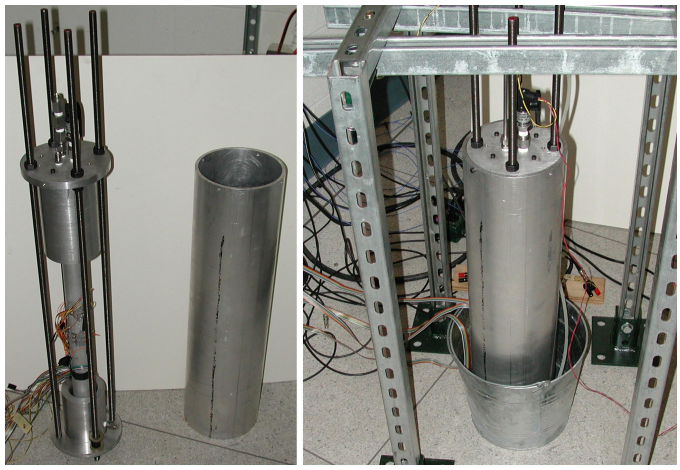

Figure 4: Tube assembly for hydraulic oil loading and gaseous nitrogen loading. Left: assembly separated from the blast shield. Right: with the blast shield. The flanges used in the hydraulic oil and nitrogen loading were the same ones as those in detonation loading.

iments. The ends of the flanges were capped, threaded rods and nuts were used to counter the resulting hydrostatic axial force, and the assembly was fixed vertically rather than clamped down on a table.

2.3 Instrumentation

The velocity and pressure of the detonation wave were measured by PCB piezo-electric pressure transducers. The pressure transducers were mounted 0.406 m apart in the detonation tube.

Micro-Measurements strain gages and crack detection gages were bonded to the external surface of the tubes to measure circumferential strain and crack arrival times, respectively. Their locations are shown in Fig. 5. Figure 6 shows a photograph of the strain gages and crack gages. Dow Corning 3145 RTV was used to protect the leads from premature destruction due to the blast wave. The Trig-Tek amplifiers that amplified the signals from the Wheatstone bridges had a bandwidth of 100 kHz.

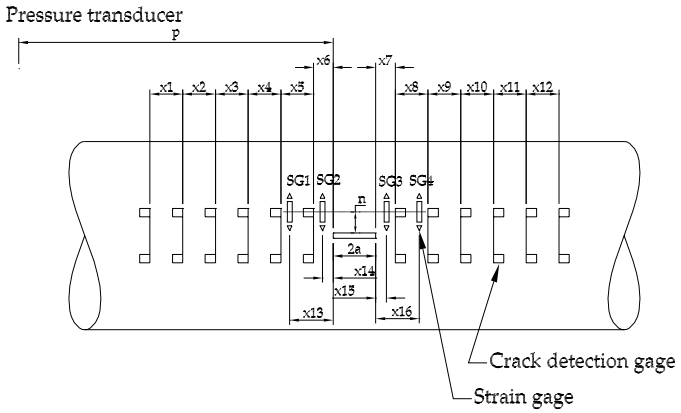

Figure 5: Schematic for crack detection gages and strain gages. In the detonation case, "pressure transducer" refers to the PCB transducer on the initiator detonation tube closest to the specimen tube.

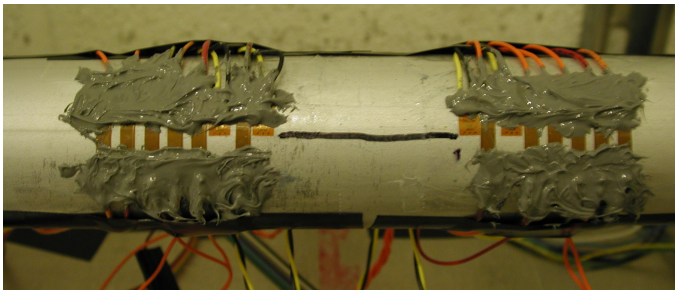

Figure 6: Photograph of crack detection gages and strain gages. The surface notch was marked in black with a pen.

In the detonation experiment, the spark and data acquisition system was triggered by a Stanford Research Systems digital pulse generator. The pressure traces, strain history, and crack arrival times were digitized with Tektronix oscilloscopes. The detonation experiment was recorded at a rate of 2.5 megasample per second, while the gaseous nitrogen and hydraulic oil experiments were recorded at a rate of 1 megasample per second. The data were transferred into a computer through a LabVIEW program.

In the gaseous nitrogen and hydraulic oil experiments, one of the crack detection gages was placed close to the surface notch tip to trigger the data acquisition system. (This trigger gage is not shown in Fig. 5.) The pressure was recorded with an Omega PX4100-3KGV pressure transducer attached to one of the endcaps.

	Detonation	Nitrogen	Oil
x1	-	5.41	-
x2	-	5.54	-
x3	-	4.95	-
x4	4.95	5.21	-
x5	9.40	9.75	-
x6	5.94	5.59	-
x7	5.61	5.49	-
x8	9.45	9.91	-
x9	5.08	5.36	-
x10	5.33	4.62	-
x11	5.38	5.38	-
x12	5.46	5.28	-
x13	12.2	12.0	12.1
x14	2.95	2.77	2.59
x15	2.92	2.79	7.85
x16	12.0	12.2	16.9
p	563	285	285
n	1.3	1.3	1.3
2a	38.1	37.4	37.5

Table 2: Crack detection gage and strain gage locations (all dimensions are in mm).

In the gaseous nitrogen experiment, nitrogen was supplied to the tube assembly from a liquid nitrogen tank via a pressure regulator and an electro-pneumatic valve. The pressure was slowly increased by turning a lever on the regulator. Upon rupture, the electro-pneumatic valve was closed by a manual switch.

In the hydraulic oil experiment, an SFX PowerTeam handpump was used to pressurize the tube assembly with SFX PowerTeam no. 9638 hydraulic oil.

3 Results and Discussion

3.1 Detonation-Driven Fracture

Of the three cases presented, the detonation case is the most complex since the internal loading depends on time and varies with position even prior to fracture and crack propagation. Additional details about the detonation-induced fracture process are given by Chao and Shepherd (2002). That study was carried out with specimens identical to the present study. The threshold for tube rupture was determined as a function of flaw size and nominal load amplitude. Dynamic amplification of peak strains and bulging of the region surrounding the flaw were identified as key issues in establishing a rupture criterion. Cracks were observed to propagate in a helical fashion for low amplitudes and short flaws. For higher amplitudes and longer flaws, crack bifurcation was observed in addition to helical paths.

Figure 7 presents a simplified view of the initial stages that is useful for strain and crack data interpretation. The x-t diagram illustrates the inception and propagation of cracks originating in the notch. For simplicity, only one fracture initiation site (and hence a unique rupture time) is shown in Fig. 7. Not shown are the three-dimensional gasdynamics of the interaction between the Taylor wave following the detonation, expansion waves created by the breached portions of the tube, and also from the open aft end of the tube. The crack curving at later stages cannot be treated in this diagram.

The detonation wave is the fastest process, giving it the most shallow slope in the x-t diagram. As it passes the notch, the stress intensity factor at the notch builds up with the hoop stress, and the notch develops into a through-wall crack. It takes a finite amount of time from the arrival of the detonation wave to the development of a through-wall crack, and we call this the 'rupture time.' The through-wall crack spreads both ways in the upstream and the downstream direction and finally propagates into the un-notched portions of the tube wall. Since the cracks are running predominantly in mode-I through aluminum, they are much slower than the detonation wave. The cracks propagating inside the notch rupture a ligament that is 37% of the tube wall and has higher stresses than the main tube wall. The cracks within the flaw, therefore, have higher stress intensity factors and accelerate to higher speeds than the main cracks that propagate along the thicker tube wall. It will be seen later, in Section 3.6, that the crack arrival times measured in these experiments fall on this slower portion of crack propagation because the crack detection gages were mounted outside the notch.

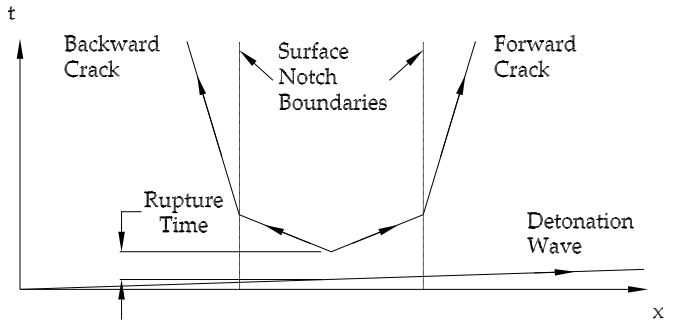

Figure 7: Hypothetical x-t diagram of a preflawed, rupturing detonation tube.

3.2 Pressure Loading

For the detonation experiment, the mixture was stoichiometric ethylene-oxygen (C_2H_4+$3O_2$) at an initial pressure of 1.8 atm and room temperature. The pressure peak recorded by the pressure transducer is not reliable due to noise, the three-dimensional structure of the detonation wave front, and the finite size of the pressure transducer. For this reason, computed values of the Chapman-Jouguet (CJ) pressure were used to characterize the detonation. The calculated (Reynolds 1986) CJ pressure and wave speed are 6.2 MPa and 2390 m/s. The detonation pressure history recorded on the pressure transducer closest to the flange is shown in Fig. 8. This is a typical gaseous detonation pressure trace with the initial CJ point (around 0.6 ms) coinciding with the shock front, immediately followed by a Taylor expansion wave. After the end of the Taylor expansion, there is a short plateau (1.2 to 1.6 ms) followed by the expansion wave that came from the rupture and the open end of the tube. The detonation wave speeds were measured just before entering the specimen tube and are typically within 5% of the computed values.

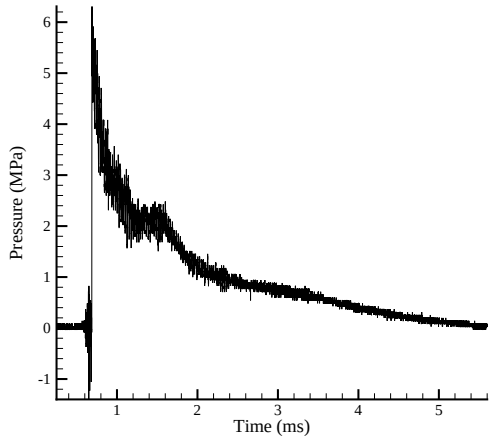

Figure 8: Pressure history for a detonation experiment. Time $t = 0$ corresponds to the spark in the initiator detonation tube. The CJ pressure is 6.2 MPa. The ringing in pressure prior to the CJ state was due to elastic waves that propagated along the detonation tube wall ahead of the detonation wave and excited an uncompensated acceleration response in the pressure transducer.

The burst pressures of the gaseous nitrogen experiment (5.5 MPa, see Fig. 9) and hydraulic oil experiment (6.0 MPa, see Fig. 10) were only slightly lower than the CJ pressure of the detonation experiment. However, loading and unloading rates were quite different in the three cases. The pressure was increased very slowly in the static tests and the loading rate was zero for all practical purposes in the nitrogen and hydraulic oil experiments. The pressure transducer used in the nitrogen and hydraulic oil experiments was too slow (response time of 10 ms) to capture the initial fast pressure transients during rupture (the original intention being only to capture the burst pressure). However, one can still get a rough idea of the depressurization rate. In the hydraulic experiment, it took about 15 ms to drop to about 3 MPa, while in the nitrogen experiment, it took as long as about 25 ms. In the detonation experiment, the loading is essentially complete after a few μs, and the unloading occurs in two stages. Immediately following the detonation, it took only about 0.4 ms for pressure to drop from 6 MPa to 2 MPa and then a slower decay occurs over the next 5 ms. Note that these three pressure traces were recorded at different locations with very different gages so that the comparison is only qualitative.

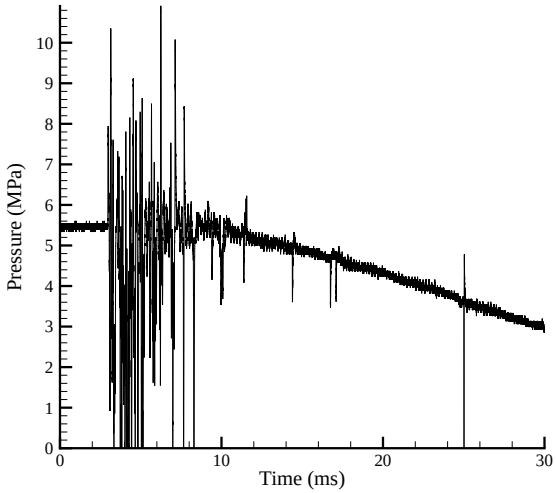

Figure 9: Pressure history for a gaseous nitrogen experiment. Time $t = 3$ ms corresponds to the crack passing the trigger wire. The burst pressure is around 5.5 MPa. The pressure spikes seen from 4 ms to 10 ms, immediately after rupture, are either unresolved waves in the gas or else vibration-induced artifacts.

3.3 Fracture Behavior as a Function of Loading

As can be seen in the post-test specimens in Figs. 11 (hydraulic oil), 12 (detonation), and 13 (gaseous nitrogen), the

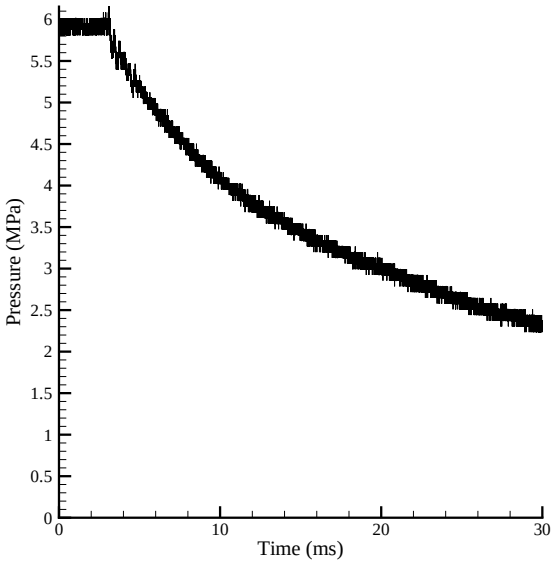

Figure 10: Pressure history of a hydraulic oil experiment. Time $t = 3$ ms corresponds to the crack passing the trigger wire. The burst pressure is about 6 MPa.

fracture behavior is a strong function of the applied loading.

In Fig. 12, the detonation wave traveled from left to right. As the wave propagated past the surface notch, the hoop stress opened the notch into a through-wall crack. Two crack fronts then propagated–one in the forward direction (i.e., same direction as the detonation wave) and one in the backward direction (i.e., in the opposite direction of the detonation wave). We will refer to these two crack fronts simply as the "forward" and "backward" cracks. Both the forward and backward cracks propagated straight for some distance, then turned, ran helically around the tube, and were arrested.

Under initially static gaseous loading with nitrogen, the cracks ran straight and did not arrest until they propagated to the supports (Fig. 13). Both cracks began to turn as they approached the supports.

In the experiment with hydraulic oil, the cracks were arrested almost immediately after they left the notch (Fig. 11). The cracks were so short that they did not run past enough crack detection gages for crack arrival time measurements (see the zoom-in insert of Fig. 11). This behavior is relatively benign and in stark contrast to the extensive fractures observed with the static nitrogen or detonation tests. These observations support the standard practice (ASME 2000) of hydrostatic pressure testing using liquids as opposed to pneumatic testing using gases.

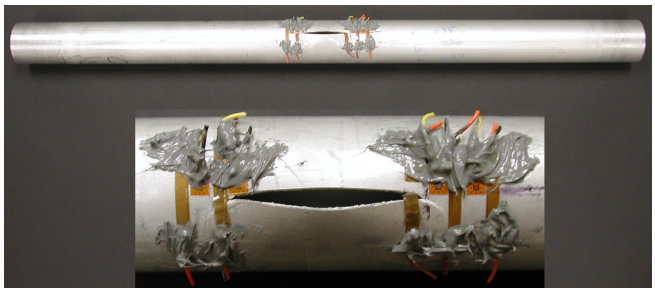

Figure 11: Post-test specimen of hydraulic experiment.

3.4 Fractographs

Light microscope pictures of fracture surfaces were taken and some of these are shown for detonation and nitrogen experiments in Figs. 12 and 13, respectively. The magnification was 30X with a Leica GZ4 light microscope which was coupled to a Nikon Coolpix 990 digital camera. The natural scale in these photos is the wall thickness of the tubes, which is 0.89 mm.

Two types of fractographs can be discerned in the detonation experiment. In this shot, both the forward and backward cracks first propagated straight for some distance, turned helically, and were arrested. Arrows next to the fractographs indicate the direction of propagation for the detonation waves and the cracks. The approximate locations on the tube where these fractographs were taken and the location of the initial notch are also shown.

The first type is shown in Fig. 12 (a) and (b). These fracture surfaces are along the straight portion of the cracks. They are relatively rough because 1) they were caused by the predominantly mode-I (opening mode) fracture and 2) the specimen was ductile, being above its transition temperature. Since the wall was thin, the fracture surfaces were, in general, slanted at 45 degrees to the specimen's surfaces and were composed almost entirely of shear lips. This is generally known as the 'thickness effect' in fracture mechanics (Kanninen and Popelar 1985).

The second type, less frequently reported in the literature, is shown in Fig. 12 (e) and (f). These fracture surfaces are along the curved portion of the cracks. They are relatively smoother than the fracture surfaces of the straight portion of cracks. The cracks have turned helically along the tube, and the fracture was predominantly mode-III (tearing mode) due to the large outward dynamic motion of the flaps. On some fracture surfaces, shallow striations that are almost perpendicular to the crack path can be seen, such as those in Fig. 12 (e) and (f).

The fracture surfaces of the gaseous nitrogen experiment are less distinctive from one another because the fracture

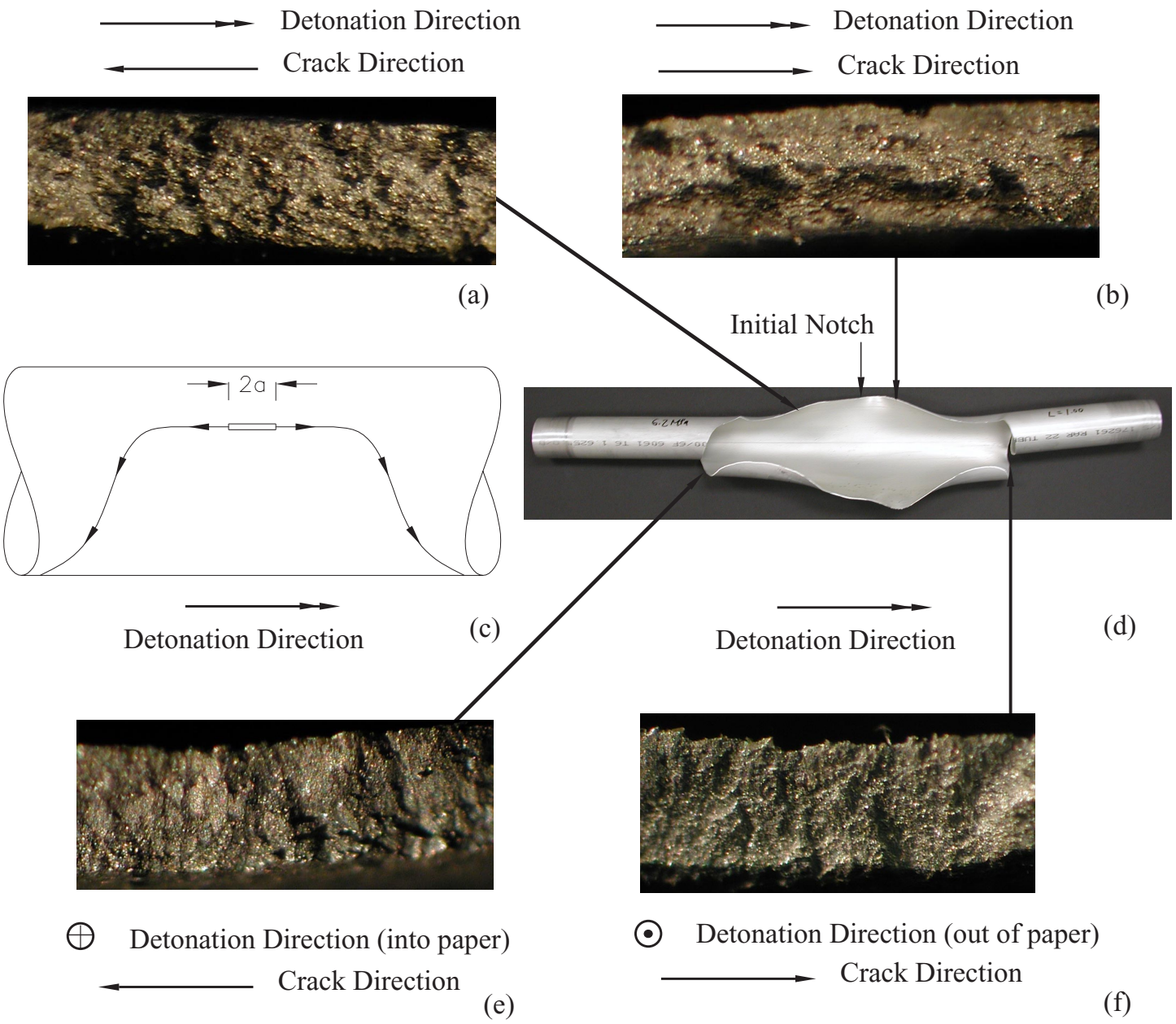

Figure 12: Fractographs, post-test specimen, and crack path schematic for a tube fractured under detonation loading.

mode stayed the same throughout the course of crack propagation. Nonetheless, the fracture surfaces farther from the notch tend to be somewhat smoother than those near the notch.

3.5 Strain Response

Internal pressure creates the stresses and associated strain fields that initiate cracks and sustain crack growth. Strain gages mounted on the tube surface were used to record the dynamic variation of the strain during those events.

Figures 14, 15, and 16 show the strain response of the specimen tubes within one or two milliseconds of rupture. In the detonation and gaseous nitrogen experiments, the strain gages and crack gages were located at the straight portions of the propagating cracks. The average crack speeds calculated from arrival times between consecutive crack gages are plotted in Figs. 18 and 19. The strain rates

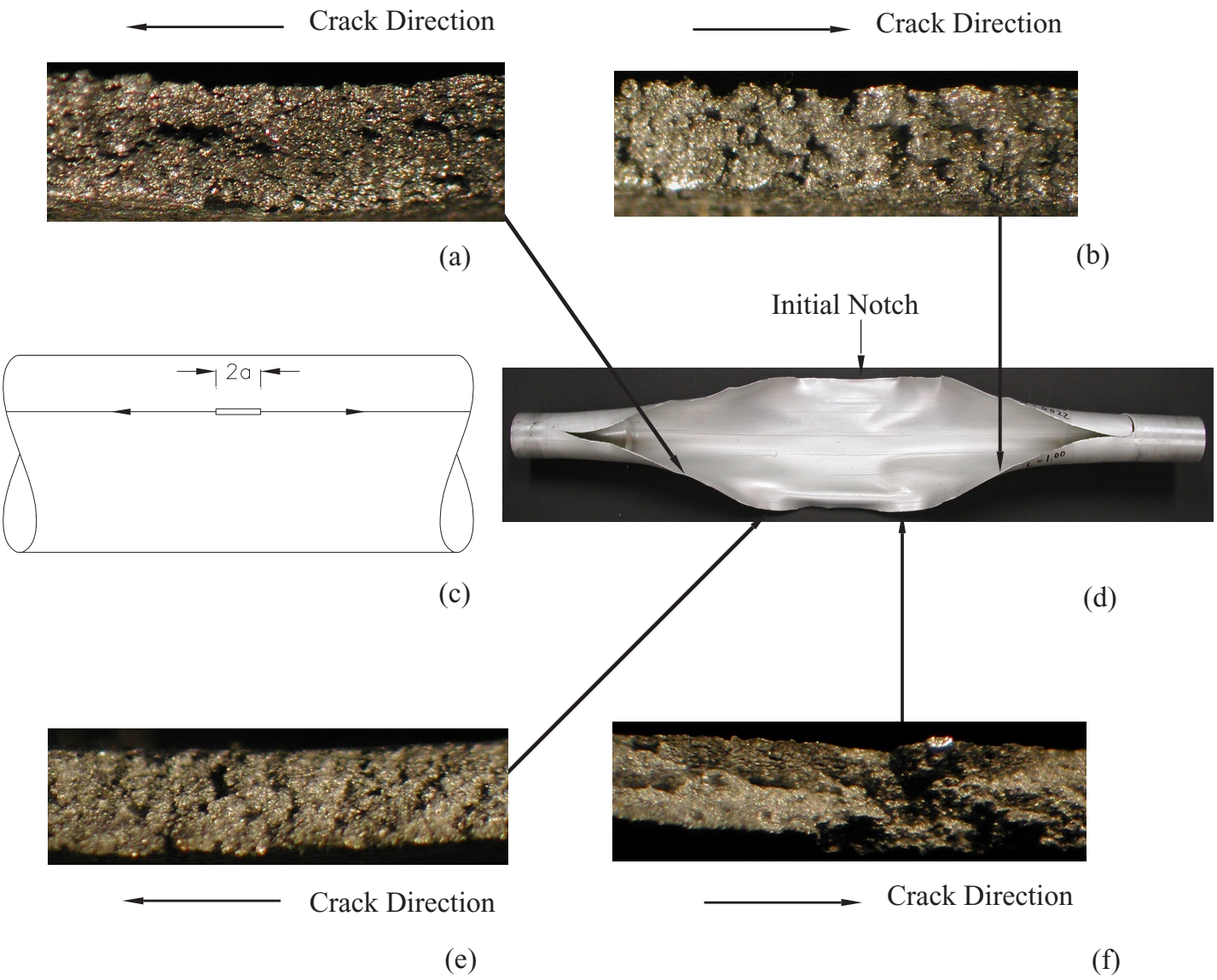

Figure 13: Fractographs, post-test specimen, and crack path schematic for a tube fractured under gaseous nitrogen loading.

ranged typically from 10^2 s^{-1} to 10^3 s^{-1}.

The initial hoop strain patterns of the gaseous nitrogen and hydraulic oil experiments are qualitatively similar. They are on different time scales, but the strain histories of corresponding gages in the two experiments are generally of the same shape. In both plots, all strains start near the burst pressure. The initial drop in strain results from both the depressurization of the fluid and the motion of the flaps of material created by the propagating crack. The flaps fold outward and are hinged about the crack front; this motion compresses the material ahead of the crack. This hinge effect causes a drop in strain at a distance ahead of the crack and is common in flat-plate mode-I fracture. Since SG2 and SG3 were closer to the notch, as the cracks ran by, the crack tip stress concentrations along with the significant residual internal pressure caused sharp strain peaks. SG1 and SG4 were further from the notch, and one does not see such high strain peaks because the internal pressure had already been relieved quite significantly. Another point of interest is that although SG2 and SG3 in the hydraulic oil experiment are schematically symmetric about the notch, their signals look dissimilar because their actual locations were not symmetric about the notch (Table 2).

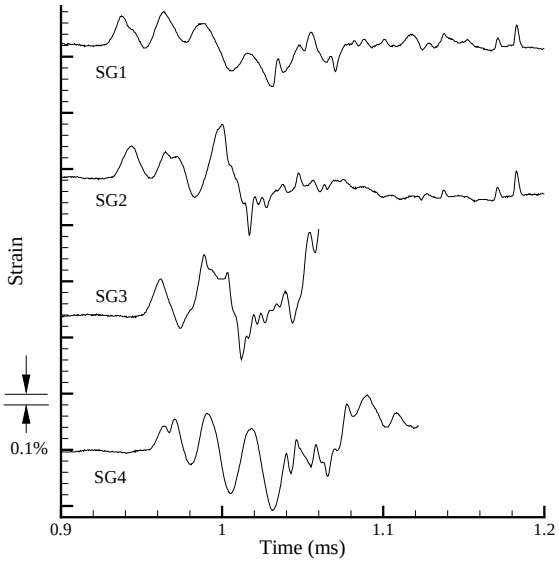

Figure 14: Hoop strains in a detonation experiment. Time $t = 0$ corresponds to the spark in the initiator detonation tube. The initial strain is zero in all cases and displaced for the purposes of display.

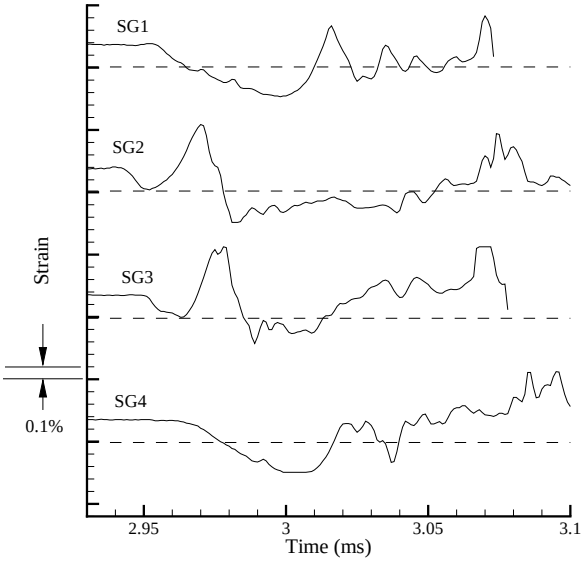

Figure 15: Hoop strains in a gaseous nitrogen experiment. Time $t = 3$ ms corresponds to the crack passing the trigger wire. Each strain begins at a value corresponding to the burst pressure. Dashed lines indicate zero strain at the respective strain gages. Slight clipping occurred for signal SG3.

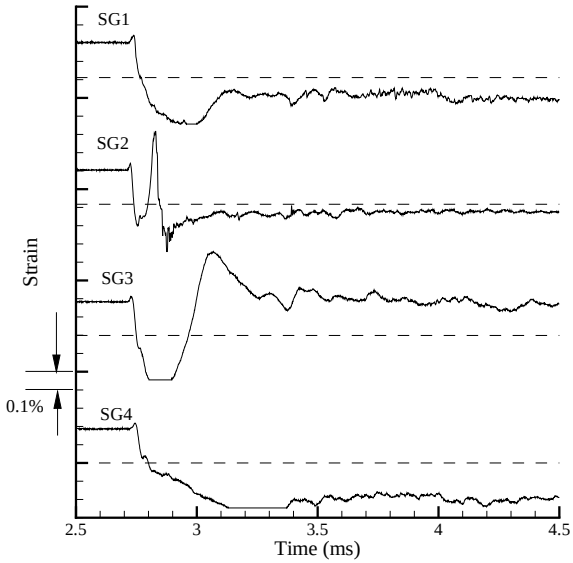

Figure 16: Hoop strain of a hydraulic oil experiment at times close to crack initiation. Time $t = 3$ ms corresponds to the crack passing the trigger wire. Each strain begins at a value corresponding to the burst pressure. Dashed lines indicate zero strain for each respective strain gage. Slight clipping occurred in signals SG3 and SG4.

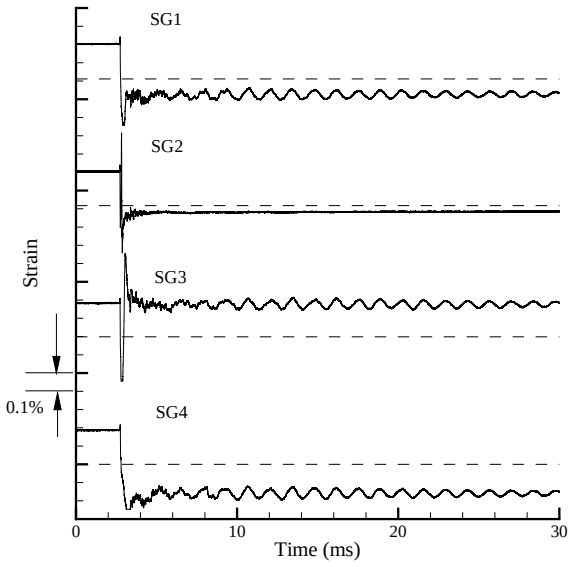

Figure 17: Hoop strains for a hydraulic oil experiment at long times compared to crack opening.

3.5.1 "Static" Loading versus "Dynamic" Loading

So far, we have referred to gaseous nitrogen and hydraulic oil loading as "static" and detonation loading as "dynamic."

This distinction is no longer valid once the crack opens because both the gaseous nitrogen and hydraulic oil unload dynamically. Nonetheless, there are major differences between the strain response caused by a traveling detonation load and that caused by nitrogen or oil decompression.

The first important difference is the magnitude of the initial strain. The initial strain of the nitrogen and oil experiments is about 0.2%, equal to the static cylindrical shell prediction using the burst pressure. The magnitude of the first strain cycle (uncontaminated by stress concentrations because crack has not yet arrived) of the detonation experiment is about 0.3%, giving a dynamic amplification factor (ratio of dynamic strain to static prediction) of 1.5 using the CJ pressure. The traveling detonation load caused stresses and strains higher than static predictions. The steady-state Tang (1965) model predicts a dynamic amplification factor of 2 for the present situation. An extensive discussion of dynamic amplification factors as a function of detonation loading can be found in Beltman and Shepherd (2002). In that study, it was shown that the length of the tube and the location of flanges can have a significant effect on the actual values of the amplification factor. If the amplification factor must be known exactly, then either detailed measurements or finite-element simulations are necessary.

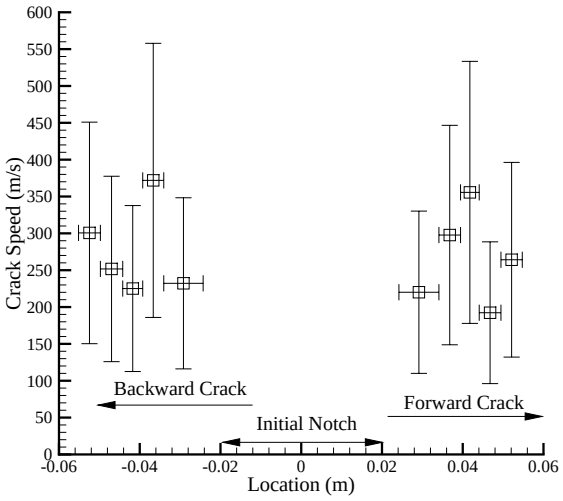

Figure 18: Crack speeds for a tube under gaseous nitrogen loading.

The second important difference is the fatigue-like, oscillatory nature of the strain response caused by detonation load that is not observed in the static load cases. The first two or three cycles of strain that are shown by the strain gages on Fig. 14 show typical elastic strains of flexural waves excited by a detonation wave that traveled between the first two critical wave speeds of the structure. While the reader is referred to Beltman and Shepherd (2002) and Chao and Shepherd (2002) for a more detailed discussion of detonation-induced flexural waves in tubes, several points are worth mentioning here. First, the strain front coincides with the detonation wave front. Second, the frequencies of the strains correspond closely to Tang's (1965) theoretical steady-state frequency, which is 50 kHz for this tube. Third, since the flexural waves were dispersive and the detonation wave was traveling above the first critical wave speed, precursor waves at frequencies over 1 MHz would travel ahead of the strain signals associated with the main flexural wave. The reasons that they are invisible are that 1) they are of small amplitude compared to the main signal, and 2) the amplifiers, having a bandwidth of 100 kHz, attenuated the high frequency precursors.

The third important difference is that the loading and unloading have a preferred direction in the detonation case. The detonation propagates along the tube, creating a spatially-dependent stress field in the tube, sweeping over the notch, and setting up a flow field behind the wave. The crack initiation process will be asymmetric due to the interaction of the elastic waves created by the detonation passing over the notch and the strain field created by the fracture process itself. The expansion waves in the detonation interact with the flow field so that the subsequent stress field in the tube will be different upstream and downstream of the notch. This asymmetry will be reflected in an asymmetric fracture process. The results are the higher stresses and higher stress intensity factors associated with the forward crack. This is evidenced in the consistently higher crack speeds of the forward crack than those of the backward crack (Fig. 19). The asymmetry was also demonstrated in a related study by Chao and Shepherd (2002) on the fracture behavior as a function of initial flaw length using similar specimens. For short initial flaws, both the forward and backward cracks propagated helically without bifurcation. When the initial flaw size was increased, the forward crack bifurcated while a single backward crack propagated helically. This case was shown to be repeatable and was another indication of a higher stress intensity factor at the forward crack tip due to the asymmetry of the loading. For very long initial flaws, both cracks bifurcated.

3.6 Crack Speeds

Crack speeds deduced from crack arrival times for the gaseous nitrogen loading fluctuated between 200 to 400 m/s (Fig. 18), while those of detonation loading fluctuated between 170 to 250 m/s (Fig. 19). The error bars show upper and lower bounds. Crack speeds for hydraulic oil loading were not measured because the cracks were arrested be-

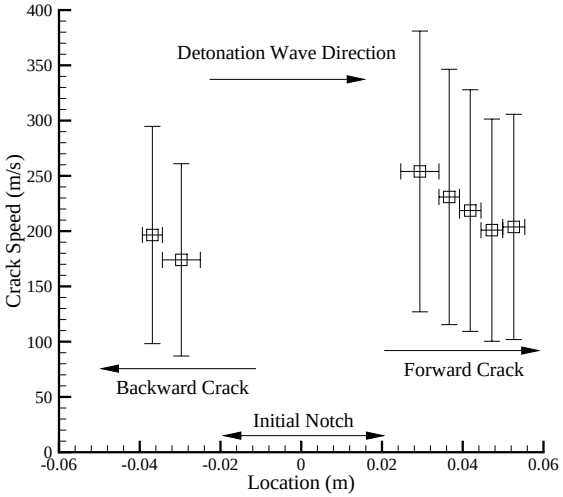

Figure 19: Crack speeds for a tube under detonation loading.

fore reaching the crack gage locations. From the measured crack speeds, it appears that the gaseous nitrogen loading provided a slightly larger crack driving force than the detonation loading. In the nitrogen case, the tube was prestressed everywhere when rupture occurred and the stress state decayed slowly in comparison to the fracture propagation time. A 200 m/s crack tip would propagate 0.3 m from the notch to the tube end in 1.5 ms, and the pressure decays a neglible amount during this time (Fig. 9). In the detonation case, only the portion of the tube behind the detonation wave was loaded and the pressure decays substantially during the time the crack tips propagate towards the ends of the tube (Fig. 8). Figures 20 and 21 are composite plots of different views of the strain, crack, and detonation trajectories in an x-t-strain space. The detonation trajectories were predicted assuming that the fracture process did not affect the detonation velocity. The detonation wave speeds were obtained from the detonation front arrival times at the pressure transducers in the detonation tube, and then extrapolating the detonation trajectory into the specimen tube.

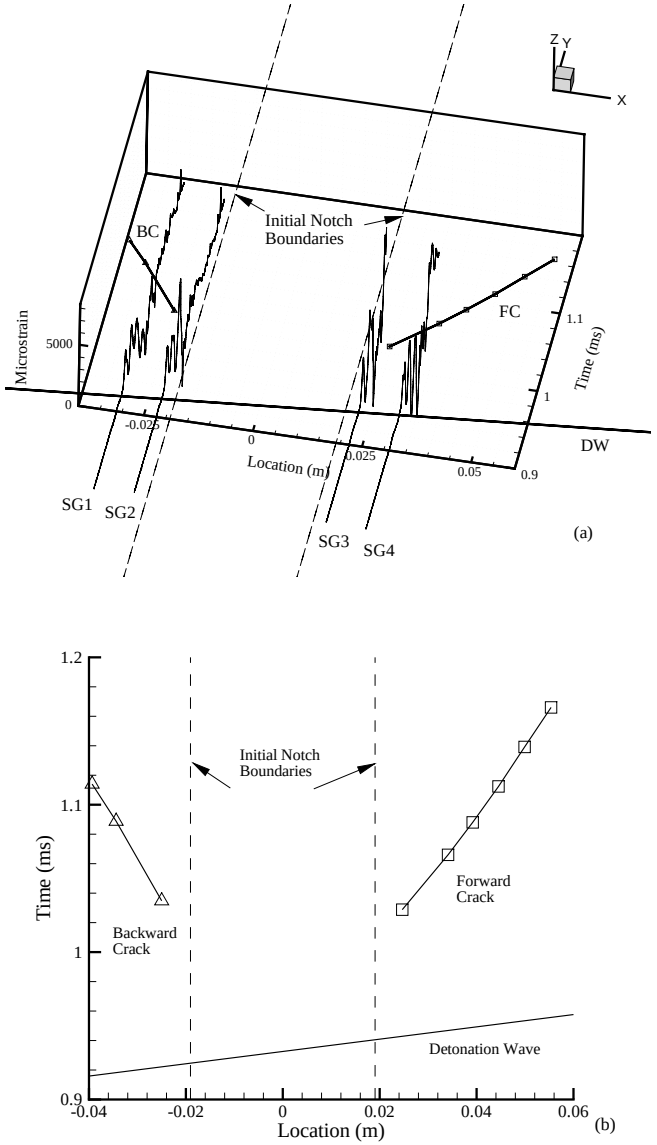

Figure 20: Two representations of the x-t-strain diagram of a detonation experiment.

4 Effect of Fluid Properties

The differences in observed fracture behavior are quite striking and most apparent when comparing the hydraulic oil loading with either of the two gas loading cases. This immediately suggests that the large difference in physical properties of gases and liquids is responsible for the differences in fracture behavior. The properties of greatest interest are specific volume v and sound speed c, which can be combined to form the isentropic compressibility

$$K_s \equiv -\frac{1}{v}\frac{\partial v}{\partial P}\bigg|_s = \frac{v}{c^2}\,. \tag{1}$$

Values of these properties have been estimated for all three fluids used in present experiments and are given in Table 3. Inspection of these values indicates a two-order-of-magnitude difference between the gas and liquid compress-

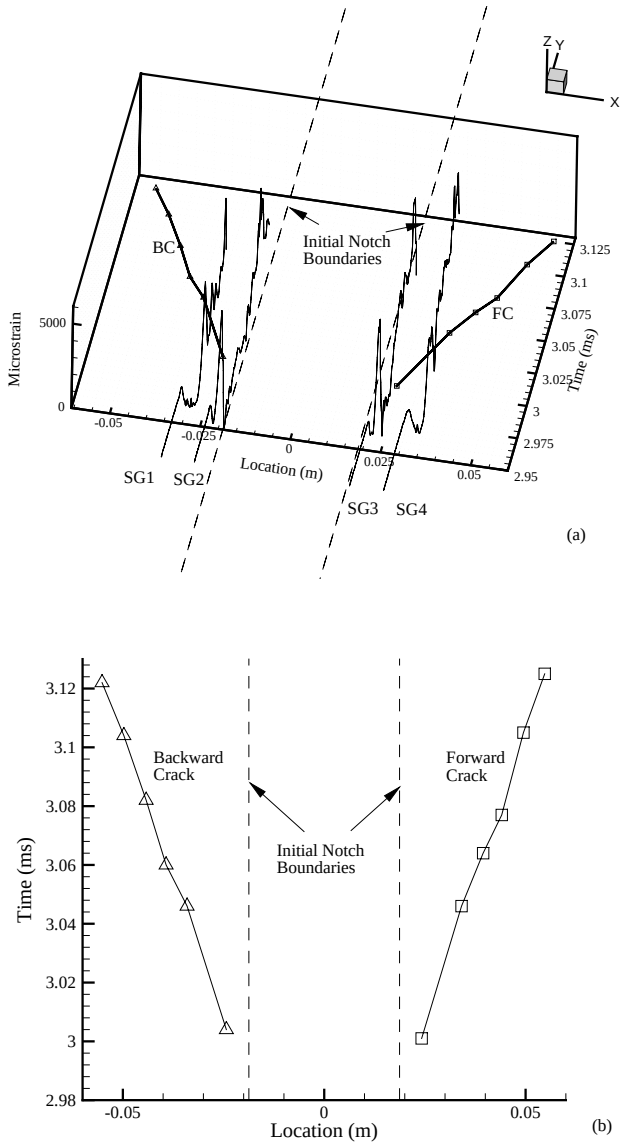

Figure 21: Two representations of the x-t-strain diagram of a gaseous nitrogen experiment.

ibility. As shown below, the main consequence of this is that a much larger (three orders of magnitude) amount of energy can be stored in the compressed gases or detonation products than in the hydraulic oil. A secondary factor is that the crack speeds are comparable to the sound speeds in the nitrogen case but a factor of 5 lower than the sound speed in the detonation products.

We have identified three principle physical processes associated with the fluid-structure interaction that will influence the fracture process. First, the pressure will begin to drop in the tube once a thru-crack has developed and fluid begins

Fluid	c (m/s)	v (m^3/kg)	K_s (m^2/N)
Detonation Products	1300	0.24	1.4×10^{-7}
Nitrogen Gas	354	0.016	1.3×10^{-7}
Hydraulic Oil	1154	0.0011	8.3×10^{-10}

Table 3: Properties of the fluids used for loading. Detonation products are evaluated at CJ state. Nitrogen is evaluated at burst pressure of 5.5 MPa and room temperature. Since the sound speed of the hydraulic oil was not available from the manufacturer, it was measured in our laboratory.

venting out of the crack opening. This will reduce the pressure in the vicinity of the crack, lowering the hoop stress in the tube and reducing the crack driving force. Second, the local reduction in pressure due to the fluid venting will propagate through the fluid as an expansion wave, the head of this wave moving at the sound speed in the static fluid and with the sum of sound and flow velocities in the moving fluid. This will reduce hoop stress near or ahead of the crack tip, reducing the crack driving force. Third, the fluid does work through plastic deformation and acceleration of the "flaps" of material created by the fracture process. The amount of work that can be done is limited by the amount of energy initially stored in the fluid. This energy can be estimated from thermodynamic principles and compared to the elastic energy in the tube as well as the energy required to create new fracture surfaces. Brief explorations of each of these issues are given in the subsequent sections.

4.1 Venting

For a small (isentropic) change in specific volume Δv, the pressure drop ΔP is

$$\Delta P = \left.\frac{\Delta P}{\Delta v}\right|_s \Delta v = \left.\frac{\partial P}{\partial v}\right|_s \Delta v = -\frac{1}{K_s}\frac{\Delta v}{v}. \qquad (2)$$

Inspection of the values in Table 3 indicates that the liquid will depressurize much more rapidly than the gases, causing the hoop stress near the original notch to rapidly decrease once the fluid starts to vent. For example, venting 0.5% of the original volume of the hydraulic oil is sufficient to drop the average pressure in the tube from 6 MPa to zero. On the other hand, venting a similar amount from the compressed nitrogen reduces the pressure only by 38 kPa, a factor of 10^2 less.

4.2 Expansion Waves

Expansion waves generated by the venting of fluid out of the crack opening will travel fastest in the detonation products

and hydraulic oil and slowest in the nitrogen (Table 3). The situation is complex in the detonation case because the fluid is moving behind the detonation wave, creating a spatially nonuniform pressure field (Beltman and Shepherd 2002). However, it is clear from the measured crack propagation speeds that the expansion waves travel 5 times faster than the crack tips and the detonation wave travels 10 times faster than the crack tips.

This means that the expansion waves travel faster than the crack tips in both the hydraulic oil and the detonation cases. This will result in a decrease in the hoop stress and decreasing crack driving force as the crack tip grows. This is one factor that causes the cracks in the detonation case to arrest early rather than propagate to the end of the tube as observed in the nitrogen case. In the nitrogen loading case, the expansion waves travel at a speed comparable to the crack tip. This suggests that the stress field ahead of the crack will be relatively unaffected by the expansion wave until the cracks arrive at the tube ends.

4.3 Energy Storage

Internal pressurization of the tubes is associated with stored energy due to the compressibility of the fluid and the elastic nature of the tube material. This stored energy will be converted into kinetic energy and internal energy of the tube, fluid contents, and surrounding air. A notional energy balance for the process of fracture and tube rupture can be written as

$$\Delta U^{elastic}_{fluid} + \Delta U^{elastic}_{solid} = \Delta E^{K.E.}_{fluid} + \Delta E^{K.E.}_{solid} + \Delta E_{plastic} + \Delta E_{fracture} + \Delta E_{dissipated} \ . \quad (3)$$

Similar energy balance was considered by Emery et al. (1986) and Poynton et al. (1974). One of the main differences between the present study and the other two studies is the energy associated with the fluid. While the other two considered only the part of fluid energy which does work on the fracturing pipe by assuming a pressure decay profile and a flap displacement pattern, the present study considers maximum energy that is stored in the fluid from a thermodynamic point of view. The energy balance above represents a total energy approach and is different from those that aim that deriving the crack driving force, such as ones by Freund (1998) and Kanninen and Popelar (1985).

The terms on the left hand side account for the elastic strain energy stored relative to the reference configuration of the tube and fluid at atmospheric pressure. The terms on the right include kinetic energy of the tube, energy for large scale plastic deformation of the flaps, energy required for the fracture process, and dissipation due to heat transfer, etc., after rupture. Only a few of these terms will be estimated in this study.

Thermodynamic considerations can be used to provide upper bounds for stored energy in the fluid. For nitrogen, a perfect gas model $Pv = RT$ can be used and the stored energy estimated by considering isentropic expansion from the initial state (1) to the final state (2) at the pressure of the surrounding atmosphere

$$\Delta s = c_p \ln \frac{T_2}{T_1} - R \ln \frac{P_2}{P_1} = 0 \ , \ c_p = \frac{\gamma R}{\gamma - 1} \ , \ \frac{c_p}{c_v} = \gamma \ . \quad (4)$$

The compressibility varies inversely with pressure for an ideal gas

$$K_s = \frac{1}{\gamma P} \quad (5)$$

and this has to be taken into account when computing the stored energy for a gas. The simplest way to do that is to use the first law of thermodynamics and evaluate the work done as the change in internal energy during the expansion from state 2 to 1

$$\Delta u = c_v (T_1 - T_2) \ , \quad (6)$$

with T_2 computed from Eq. 4. The energy change per unit mass during isentropic expansion of gaseous nitrogen is then

$$\Delta u^{elastic}_{nitrogen} = \frac{P_1 v_1}{\gamma - 1} \left[1 - \left(\frac{P_2}{P_1} \right)^{\frac{\gamma - 1}{\gamma}} \right] \ . \quad (7)$$

A similar computation can be carried out for the high-pressure, hot gases behind the detonation wave, taking into account the kinetic energy in the products (Cooper and Shepherd 2002).

The stored energy in the hydraulic oil can be computed from the first law of thermodynamics to be

$$\Delta u^{elastic}_{oil} = \int_{v_1}^{v_2} P dv \ . \quad (8)$$

Since the volume change of the liquid is quite small for the pressures we are considering, it is easier to work with the pressure and write this as

$$\Delta u^{elastic}_{oil} = - \int_{P_1}^{P_2} v K_s P dP \ . \quad (9)$$

This can be simplified by assuming that the compressibility is constant so that by using the definition of K_s (Eq. 1) and integrating to obtain the volume dependence on pressure

$$v = v_1 \exp(-K_s (P - P_1)) \quad (10)$$

Expanding in powers of the argument, we have

$$v \approx v_1 (1 - K_s (P - P_1) + \mathcal{O}(K_s (P - P_1))^2 \ . \quad (11)$$

Retaining only the first term in this expansion, we can carry out the integration in Eq. 9 to obtain

$$\Delta u_{oil}^{elastic} \approx v_1 K_s \left(\frac{P_1^2 - P_2^2}{2} \right). \quad (12)$$

For comparison, it is better to work on a unit volume basis since the tubes contain a fixed volume of fluid. For the gaseous nitrogen, this will be

$$\frac{\Delta U_{nitrogen}^{elastic}}{V} = \frac{P_1}{\gamma - 1} \left[1 - \left(\frac{P_2}{P_1} \right)^{\frac{\gamma-1}{\gamma}} \right] = 10 \text{ MJ/m}^3 . \quad (13)$$

The Fickett-Jacobs thermodynamic cycle computation of Cooper and Shepherd (2002) for C_2H_4+3O_2 detonation products yields

$$\frac{\Delta U_{detonation}^{elastic}}{V} = 7.2 \text{ MJ/m}^3 . \quad (14)$$

For the hydraulic oil, this will be

$$\frac{\Delta U_{oil}^{elastic}}{V} \approx K_s \left(\frac{P_1^2 - P_2^2}{2} \right) = 15 \text{ kJ/m}^3 . \quad (15)$$

In these calculations, it was assumed that $\gamma = 1.4$, $P_1 = 6$ MPa, and $P_2 = 0.1$ MPa. The energy stored in the gaseous nitrogen per unit volume is 10^3 times larger than that of the oil.

The elastic energy stored in the tube can be estimated by assuming that the extensions were all in the radial direction. This is a reasonable approximation for most of the tube since the ends were a slip-fit into the flanges, and the pressure on the endplates was balanced by threaded rods. If the hoop stress was the only principal stress, the elastic energy stored per unit volume in the solid before rupture is

$$\frac{1}{2}\sigma\epsilon = \frac{\Delta P^2 R^2}{2Eh^2} , \quad (16)$$

where $\Delta P = P_1$ - P_2. The rate at which the tube's elastic energy is released during fracture requires an analysis based on the equations of motion and computation of the energy flux into the crack tip. Lacking this, as a first estimate, we will assume that all the elastic energy in a ring of material with volume $(2\pi Rh\Delta a)$ behind the crack tip is released upon crack arrival. On this basis, the rate of elastic energy released per unit crack advance is

$$\frac{\Delta U_{solid}^{elastic}}{\Delta a} \approx \frac{\Delta P^2 R^2}{2Eh^2}(2\pi Rh) = \frac{\pi \Delta P^2 R^3}{Eh} = 16 \text{ J/m} \quad (17)$$

for $\Delta P = 6$ MPa. From a fracture mechanics point of view (Broek 1997), only a fraction of this energy will be used to create fracture surface because there are many other mechanisms for absorbing the stored energy in the fluid and tube. The energy requirement related to crack resistance (per unit crack advance) is

$$\frac{\Delta E_{fracture}}{\Delta a} \geq hG_c \quad (18)$$

where G_c is the fracture propagation toughness. Physically, this means that for fracture to occur, the rate of energy flow into the crack tip must be equal to or greater than the fracture propagation toughness. Although G_c was not measured for this study, it can be estimated (Broek 1997) from the mode-I critical stress intensity of Al6061-T6

$$hG_c \approx h\frac{K_{Ic}^2}{E} = 12 \text{ J/m} . \quad (19)$$

The energy approximations above are summarized in Table 4. The energy stored in the fluid has been converted to energy per unit tube length to allow a more meaningful comparison with the elastic energy and fracture energy. It is clear that from energy considerations, the cracks were significantly shorter for oil loading than nitrogen loading because for the nearly incompressible liquid, a modest amount of stored energy was available to be converted to energy for driving a crack. For the very compressible gases, the stored energy was much larger, by a factor of 10^3, and ample energy was available to create fracture surfaces.

Energy	Det. (J/M)	N_2 (J/m)	Oil (J/m)
Fluid	9.4×10^3	13×10^3	20
Solid	16	16	16
Fracture	12	12	12

Table 4: Fluid energy stored per unit tube length compared to elastic solid energy release per unit crack advance and fracture energy expenditure per unit crack advance.

Conclusion

Experiments were conducted on thin-walled and preflawed aluminum 6061-T6 tubes. Three different methods of internal loading were applied: gaseous detonation, gaseous nitrogen at room temperature, and hydraulic oil. The pressure magnitudes of the three experiments were controlled to be approximately the same. Significantly different fracture behavior, crack speeds, and strain response were observed. The static nitrogen case resulted in the most damage to the specimen, while the hydraulic oil resulted in the least damage. Cracks propagating for the entire length of the specimen were observed for the nitrogen loading, cracks that propagated approximately half that distance were observed

for detonation loading, and cracks that arrested immediately were observed for the hydraulic oil loading.

The differences in the rupture behavior were examined in terms of the physical parameters of the fluids and their influence on the physical processes involved in the rupture event. The key role of fluid compressibility was highlighted. The striking difference between the results of tests with hydraulic oil and high-pressure gases can be explained in terms of stored energy in the fluid relative to the energy required for fracture surface generation. A secondary role of sound speed in determining expansion wave propagation was identified as probably being responsible for the observed differences between nitrogen and detonation products. Fluid compressibility is also a significant factor in the venting process that determines the pressure history once the crack begins to open.

Acknowledgments

The authors thank W. G. Knauss and G. Ravichandran for their helpful discussions and additionally thank Prof. Knauss for the loan of the hydraulic pump and hose. Our thanks also go to A. J. Rosakis and D. D. Anderson for lending us the circuit for conditioning crack detection gage signals. This research was sponsored in part through the Office of Naval Research (ONR) contract N00014-99-1-0744 and by the US DOE through the Caltech ASCI project.

References

ASME, 2000. *ASME Boiler and Pressure Vessel Code - An International Code*. New York, NY: The American Society of Mechanical Engineers. Section VIII, Div. 1 (Part UG-100), Div. 2 (Article T-4).

Beltman, W., E. Burcsu, J. Shepherd, and L. Zuhal, 1999. The structural response of cylindrical shells to internal shock loading. *Journal of Pressure Vessel Technology 121*, 315–322.

Beltman, W. and J. Shepherd, 2002. Linear elastic response of tubes to internal detonation loading. *Journal of Sound and Vibration 252*(4), 617–655.

Broek, D., 1997. *Elementary Engineering Fracture Mechanics* (Fourth revised ed.). Kluwer academic publishers.

Chao, T. W. and J. E. Shepherd, 2002. Fracture response of externally-flawed cylindrical shells to internal gaseous detonation loading. In *ASME Pressure Vessels and Piping Conference*. ASME.

Cooper, M. and J. E. Shepherd, 2002. The effect of nozzles and extensions on detonation tube performance. 38th AIAA/ASME/SAE/ASEE Joint Propulsion Conference and Exhibit, July 7-10, 2002, Indianapolis IN, AIAA 2002-2628.

de Malherbe, M., R. Wing, A. Laderman, and A. Oppenheim, 1966. Response of a cylindrical shell to internal blast loading. *Journal of Mechanical Engineering Science 8*(1), 91–98.

Emery, A. F., A. S. Kobayashi, W. J. Love, B. W. Place, and Y. H. Chao, 1986. An experimental and analytical investigation of axial crack propagation in long pipes. *Engineering Fracture Mechanics 23*(1), 215–226.

Folias, E. S., 1965. A finite crack in a pressurized cylindrical shell. *International Journal of Fracture Mechanics 1*, 104–113.

Freund, L. B., 1998. *Dynamic Fracture Mechanics*. Cambridge University Press.

Ives, K., A. Shoemaker, and R. McCartney, 1974. Pipe deformation during a running shear fracture in line pipe. *Journal of Engineering Materials and Technology 96*(4), 309–317.

Kanninen, M. F. and C. H. Popelar, 1985. *Advanced Fracture Mechanics*. Oxford University Press, New York.

Kiefner, J. F., W. A. Maxey, R. J. Eiber, and A. R. Duffy, 1973. Failure stress levels of flaws in pressurized cylinders. In *ASTM STP 536, Progress in Flaw Growth and Fracture Toughness Testing, Proceedings of the 1972 National Symposium on Fracture Mechanics*.

Kobayashi, A. S., A. F. Emery, W. J. Love, and Y. H. Chao, 1988. Subsize experiments and numerical modeling of axial rupture of gas transmission lines. *Journal of Pressure Vessel Technology 110*, 155–160.

Maxey, W. A., J. F. Kiefner, R. J. Eiber, and A. R. Duffy, 1971. Ductile fracture initiation, propagation, and arrest in cylindrical vessels. In *ASTM STP 514, Fracture Toughness, Proceedings of the 1971 National Symposium on Fracture Mechanics PART II*.

Poynton, W. A., R. W. E. Shannon, and G. D. Fearnehough, 1974. The design and application of shear fracture propagation studies. *Journal of Engineering Materials and Technology 96*(4), 323–329.

Reismann, H., 1965. Response of a pre-stressed cylindrical shell to moving pressure load. In S. Ostrach and R. Scanlon (Eds.), *Eighth Midwest Mechanics Conference*, pp. 349–363. Pergamon Press.

Reynolds, W., 1986. The element potential method for chemical equilibrium analysis: implementation in the interactive program STANJAN. Technical report, Mechanical Engineering Department, Stanford University.

Simkins, T., 1987, July. Resonance of flexural waves in gun tubes. Technical Report ARCCB–TR–87008, US Army Armament Research, Development and Engineering Center, Watervliet, N.Y. 12189–4050.

Tang, S., 1965, October. Dynamic response of a tube under moving pressure. In *Proceedings of the American Society of Civil Engineers*, Volume 5, pp. 97–122. Engineering Mechanics Division.

Thomas, G., 2002. The response of pipes and supports generated by gaseous detonations. *Journal of Pressure Vessel Technology 124*, 66–73.

Zhuang, Z. and P. O'Donoghue, 2000. Determination of material fracture toughness by a computational/experimental approach for rapid crack propagation in PE pipe. *International Journal of Fracture 101*(3), 251–268.